
PET Imaging of Abdominal Aortic Aneurysm with ⁶⁴Cu-Labeled Anti-CD105 Antibody Fab Fragment

Sixiang Shi*¹, Hakan Orbay*², Yunan Yang², Stephen A. Graves³, Tapas R. Nayak², Hao Hong², Reinier Hernandez³, Haiming Luo², Shreya Goel¹, Charles P. Theuer⁴, Robert J. Nickles³, and Weibo Cai^{1-3,5}

¹Materials Science Program, University of Wisconsin–Madison, Madison, Wisconsin; ²Department of Radiology, University of Wisconsin–Madison, Madison, Wisconsin; ³Department of Medical Physics, University of Wisconsin–Madison, Madison, Wisconsin; ⁴TRACON Pharmaceuticals, Inc., San Diego, California; and ⁵University of Wisconsin Carbone Cancer Center, Madison, Wisconsin

The critical challenge in abdominal aortic aneurysm (AAA) research is the accurate diagnosis and assessment of AAA progression. Angiogenesis is a pathologic hallmark of AAA, and CD105 is highly expressed on newly formed vessels. Our goal was to use ⁶⁴Cu-labeled anti-CD105 antibody Fab fragment for noninvasive assessment of angiogenesis in the aortic wall in a murine model of AAA. **Methods:** Fab fragment of TRC105, a mAb that specifically binds to CD105, was generated by enzymatic papain digestion and conjugated to NOTA (1,4,7-triazacyclononane-1,4,7-triacetic acid) for ⁶⁴Cu labeling. The binding affinity/specificity of NOTA-TRC105-Fab was evaluated by flow cytometry and various ex vivo studies. BALB/c mice were anesthetized and treated with calcium phosphate to induce AAA and underwent weekly PET scans using ⁶⁴Cu-NOTA-TRC105-Fab. Biodistribution and autoradiography studies were also performed to confirm the accuracy of PET results. **Results:** NOTA-TRC105-Fab exhibited high purity and specifically bound to CD105 in vitro. Uptake of ⁶⁴Cu-NOTA-TRC105-Fab increased from a control level of 3.4 ± 0.1 to 9.5 ± 0.4 percentage injected dose per gram (%ID/g) at 6 h after injection on day 5 and decreased to 7.2 ± 1.4 %ID/g on day 12, which correlated well with biodistribution and autoradiography studies (i.e., much higher tracer uptake in AAA than normal aorta). Of note, enhanced AAA contrast was achieved, due to the minimal background in the abdominal area of mice. Degradation of elastic fibers and highly expressed CD105 were observed in ex vivo studies. **Conclusion:** ⁶⁴Cu-NOTA-TRC105-Fab cleared rapidly through the kidneys, which enabled noninvasive PET imaging of the aorta with enhanced contrast and showed increased angiogenesis (CD105 expression) during AAA. ⁶⁴Cu-NOTA-TRC105-Fab PET may potentially be used for future diagnosis and prognosis of AAA.

Key Words: abdominal aortic aneurysm (AAA); positron emission tomography (PET); antibody fragment; Fab; CD105 (endoglin)

J Nucl Med 2015; 56:927–932
DOI: 10.2967/jnumed.114.153098

Abdominal aortic aneurysm (AAA) is a common and potentially lethal vascular disease more prevalent in men over the age of 65. It is characterized by progressive expansion and weakening of

the abdominal aortic wall (1–3). Advanced AAA usually leads to rupture, which represents a leading cause of death in the Western world. In the United States, there are approximately 30,000 deaths every year because of AAA, and 15,000 of these are related to rupture of AAA (3,4). Although the techniques for effective diagnosis and treatment of AAA are urgently needed, noninvasive imaging of AAA at the molecular/cellular level is still underexplored, which has attracted tremendous interest from the research community. Several tracers, for example, ¹⁸F-FDG (5–10), have been reported for PET imaging of AAA in previous studies. However, the reliability of conventional tracers is still under debate (11), and there is need for new and more reliable molecular targets and tracers for PET imaging of AAA.

Angiogenesis has been proven to be a pathologic hallmark of AAA in both human and animal models, and it plays an important role in the development and progression of AAA (12–15). Higher levels of neovascularization are detected at the rupture edge in aortic aneurysm, suggesting that imaging of molecules and processes involved in angiogenesis can potentially depict high-risk aneurysms (16). One important advantage of targeting angiogenesis is that rapid, persistent, and specific targeting can be achieved with different probes, which endows an excellent efficiency and imaging contrast. The endothelial cells of newly formed vessels express high levels of CD105, also known as endoglin, on their surfaces (17). We have previously demonstrated the efficacy of a CD105-targeted antibody, TRC105, for in vivo imaging of angiogenesis (18–21). Therefore, we hypothesized that CD105 could act as a promising target for imaging and even for treatment of AAA.

Our goal was to investigate a novel probe for effective targeting and imaging of AAA with excellent targeting specificity and imaging contrast. To achieve this goal, we used a ⁶⁴Cu-labeled TRC105 Fab fragment (i.e., ⁶⁴Cu-NOTA-TRC105-Fab; NOTA is 1,4,7-triazacyclononane-1,4,7-triacetic acid) as a probe for PET imaging of AAA. Compared with TRC105 full antibody, TRC105-Fab could be rapidly cleared by the kidneys with shortened circulation half-life (22), possibly resulting in superior imaging contrast in the abdominal area. To the best of our knowledge, this is the first report of AAA PET imaging with an antibody fragment–based probe.

MATERIALS AND METHODS

Chemicals

TRC105 was provided by TRACON Pharmaceuticals, Inc. Rat antimouse CD31 primary antibody was purchased from BD Biosciences. AlexaFluor488- and Cy3-labeled secondary antibodies were purchased from Jackson ImmunoResearch Laboratories, Inc. S-2-(4-isothiocyanatobenzyl)-1,4,7-triazacyclononane-1,4,7-triacetic acid

Received Dec. 15, 2014; revision accepted Mar. 31, 2015.
For correspondence or reprints contact: Weibo Cai, Department of Radiology, University of Wisconsin–Madison, Rm. 7137, 1111 Highland Ave., Madison, WI 53705-2275.
E-mail: wcai@uwhealth.org
*Contributed equally to this work.
Published online Apr. 16, 2015.
COPYRIGHT © 2015 by the Society of Nuclear Medicine and Molecular Imaging, Inc.

(p-SCN-Bn-NOTA) was purchased from Macrocyclics, Inc. Fluorescein isothiocyanate (FITC) and chelex 100 resin (50–100 mesh) were acquired from Sigma-Aldrich. PD-10 desalting columns were purchased from GE Healthcare. All other reaction buffers and chemicals were from Thermo Fisher Scientific.

Generation, Characterization, and NOTA/FITC Conjugation of TRC105-Fab

TRC105-Fab was obtained by digestion of TRC105 antibody (5 mg/mL) using immobilized papain (weight ratio, papain to TRC105 = 1:40) in a reaction buffer (10 mM disodium ethylenediaminetetraacetic acid, 20 mM sodium phosphate dibasic, and 80 mM L-cysteine hydrochloride) for 4 h at 37°C under constant stirring (22,23). Subsequently, the supernatant was collected and purified by a Sephadex G-75 size-exclusion column (GE Healthcare Life Sciences) (fractionation range, 3,000–80,000 Da) using phosphate-buffered saline (PBS) as the mobile phase. The elution from the Sephadex G-75 size-exclusion column was tested by ultraviolet absorbance at 280 nm. The purity of TRC105-Fab was evaluated by sodium dodecyl sulfate polyacrylamide gel electrophoresis (SDS-PAGE; 5% stacking gel and 8% resolving gel) (24).

As-prepared TRC105-Fab was conjugated with p-SCN-Bn-NOTA or FITC at a molar ratio of 1:10 at pH 9.0 for 2 h (22). The final products (NOTA-TRC105-Fab or FITC-TRC105-Fab) were purified by PD-10 size-exclusion columns using PBS as the mobile phase to remove unbound NOTA/FITC.

Cell Lines and Flow Cytometry

Human umbilical vein endothelial cells (HUVECs) were obtained from the American Type Culture Collection and cultured as previously described (25–27). When the cells reached approximately 80% confluence, they were harvested and suspended in cold PBS with 2% bovine serum albumin at a concentration of 5×10^6 cells/mL, incubated with FITC-TRC105-Fab or FITC-TRC105-Fab-NOTA for 30 min at room temperature, and washed 3 times with cold PBS. Subsequently, the cells were analyzed using a BD FACSCalibur 4-color analysis cytometer equipped with 488- and 633-nm lasers (Becton-Dickinson) and FlowJo analysis software (Tree Star, Inc.).

AAA Animal Models

AAA was induced by topical application of calcium phosphate in 4- to 5-wk-old female BALB/c mice (Harlan) under anesthesia (2%–4% isoflurane) as described previously (28). Briefly, the abdominal cavity was opened with a midline abdominal incision. The infrarenal region of the abdominal aorta was freed from the surrounding adipofascial tissue by gentle dissection, and a small piece of 0.5 mol/L CaCl₂-soaked gauze was applied for 10 min to the aorta followed by application of another piece of PBS-soaked gauze for 5 min. Mice in the sham group were treated only with PBS for 15 min. All animal studies were conducted under a protocol approved by the University of Wisconsin Institutional Animal Care and Use Committee.

Radiolabeling, PET Imaging, and Biodistribution Studies of NOTA-TRC105-Fab

⁶⁴Cu was produced by a PETTrace cyclotron (GE Healthcare) using the ⁶⁴Ni(p,n)⁶⁴Cu reaction. ⁶⁴Cu was diluted in 300 μL of 0.1 M sodium acetate buffer (pH 5.0) and mixed with 200 μL of NOTA-TRC105-Fab (0.4 mg/mL). The reaction was performed at 37°C for 45 min with constant shaking. The resulting ⁶⁴Cu-NOTA-TRC105-Fab was purified by PD-10 size-exclusion column chromatography, using PBS as the mobile phase. The radioactive fraction containing ⁶⁴Cu-NOTA-TRC105-Fab was collected for further in vitro and in vivo studies.

PET imaging was performed on days 5 and 12 after the induction of AAA using a micro-PET/micro-CT Inveon rodent model scanner (Siemens Medical Solutions USA, Inc.). The animals were injected

with 5–10 MBq of ⁶⁴Cu-NOTA-TRC105-Fab via the tail vein, and serial images were obtained at 0.5, 3, 6, 14, and 24 h after injection. Data acquisition, image reconstruction, and region-of-interest (ROI) analysis of the PET images were performed as previously described (22,29). After the last scan at 24 h after injection on day 12, biodistribution studies were performed to corroborate PET data. Aorta, blood, and major organs/tissues were collected and wet-weighted. The radioactivity in the tissue was measured using a γ counter (PerkinElmer) and presented as percentage injected dose per gram (%ID/g) (mean ± SD).

Ex Vivo Imaging and Histology

The infrarenal portion of the abdominal aorta was collected from the animals after euthanasia. Autoradiographic images of the collected aortas were obtained using a γ camera. The aortas were frozen and cryosectioned for histologic analysis. Hematoxylin and eosin staining was performed to observe the microscopic changes in the abdominal aortic wall, acquired by a Nikon Eclipse Ti microscope (18). Frozen tissue slices of 7-μm thickness were double-stained for endothelial marker CD31 and CD105 as previously reported (20). The slides were coverslipped with Vectashield mounting medium for fluorescence with 4',6-diamidino-2-phenylindole (Vector Laboratories, Inc.). Fluorescent images were acquired by Nikon Digital Eclipse C1 plus confocal microscope (20).

RESULTS

Generation and Characterization of TRC105-Fab

The elution profile of the TRC105-Fab showed a narrow peak in ultraviolet intensity between 16 and 18 mL, indicating a high purity (Fig. 1A). This fraction was used for further studies. A narrow band corresponding to a molecular weight of 50–55 kDa was observed in SDS-PAGE (Fig. 1B), further confirming the purity of TRC105-Fab.

Flow Cytometry

CD105 is highly expressed on HUVECs (27). Our previous studies have documented that TRC105 possesses superior binding

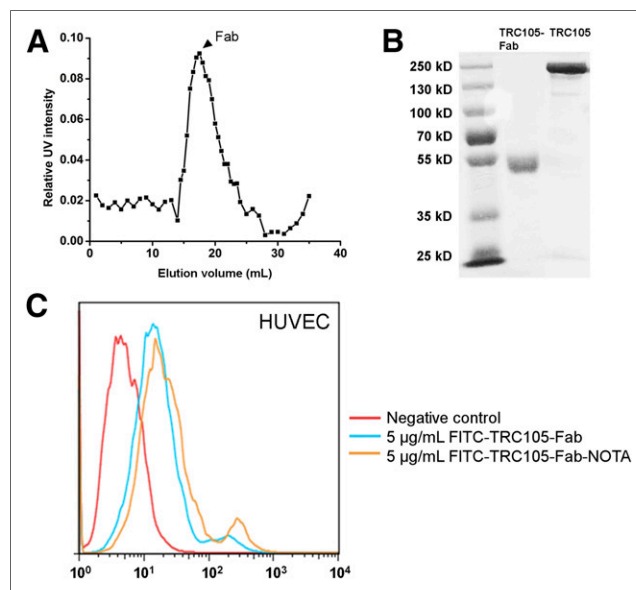


FIGURE 1. Purification and characterization of TRC105-Fab. (A) Elution profile of TRC105-Fab from Sephadex G-75 column. Arrowhead = single fraction used for further in vitro and in vivo studies. (B) SDS-PAGE of TRC105-Fab (left) and TRC105-Fab (right). (C) Flow cytometry analysis of FITC-TRC105-Fab and FITC-TRC105-Fab-NOTA (5 μg/mL) in HUVECs. UV = ultraviolet.

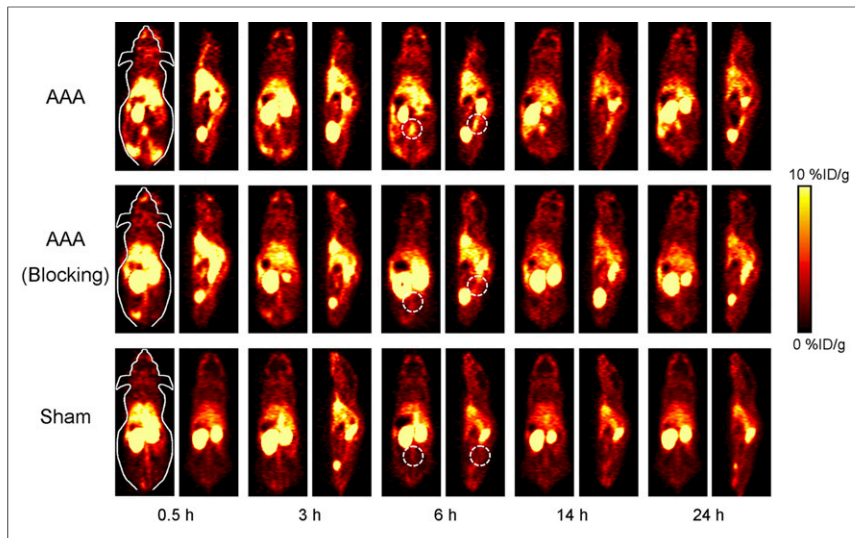


FIGURE 2. In vivo PET imaging on day 5. Serial coronal and sagittal PET images were acquired at different time points after injection of ^{64}Cu -NOTA-TRC105-Fab in AAA-induced mice, AAA-induced mice preinjected with 2 mg of TRC105 (blocking), and sham group without AAA induction on day 5 after induction.

affinity and specificity to CD105 (20,27,30). Flow cytometry was used to examine the targeting efficiency of TRC105-Fab in vitro. After the treatment with 5 μg of FITC-TRC105-Fab per milliliter, the fluorescence signal from the HUVECs exhibited an approximately 4-fold increase over the negative control (PBS-treated HUVECs) (Fig. 1C), indicating that TRC105-Fab could efficiently bind to CD105, although with a lower binding affinity than the intact

antibody. In addition, a similar increase was observed after incubating the cells with 5 μg of FITC-TRC105-Fab-NOTA per milliliter, suggesting that NOTA conjugation does not compromise the binding affinity of FITC-TRC105-Fab.

PET Imaging and Biodistribution Studies

On day 5 after AAA induction, a significantly higher tracer uptake was observed in the aortic region of the animals from the AAA group as early as 0.5 h after injection, remaining relatively stable up to 24 h after injection (9.4 ± 0.1 , 9.3 ± 0.7 , 9.5 ± 0.4 , 7.9 ± 0.5 , and 7.9 ± 0.4 %ID/g at 0.5, 3, 6, 16, and 24 h after injection, respectively; $n = 3$; Figs. 2 and 3A). On day 12, the uptake in the aortas of the animals from the AAA group was still high (8.0 ± 1.5 , 7.9 ± 1.2 , 7.2 ± 1.4 , 5.8 ± 1.0 , and 5.4 ± 1.5 %ID/g at 0.5, 3, 6, 16, and 24 h after injection, respectively; $n = 3$; Figs. 3B and 4), although a little lower in comparison to the first week.

This result suggests that ^{64}Cu -NOTA-TRC105-Fab could efficiently target AAA, and the extent of angiogenesis in AAA is stronger on day 5 than day 12, as shown by higher tracer uptake on day 5.

The in vivo targeting specificity of ^{64}Cu -NOTA-TRC105-Fab was confirmed with blocking studies on both day 5 and day 12. The signal from aorta in the blocking group was much lower than that in the AAA group and decreased significantly from 0.5 h to 24 h after injection (day 5: 7.1 ± 0.9 , 6.3 ± 0.8 , 5.5 ± 1.0 , 4.2 ± 0.4 , and 3.4 ± 0.2 %ID/g; day 12: 5.7 ± 0.8 , 4.5 ± 0.2 , 4.5 ± 0.5 , 3.1 ± 0.3 , and 3.0 ± 0.1 %ID/g at 0.5, 3, 6, 16, and 24 h after injection, respectively; $n = 3$; Figs. 2, 3A, 3B, and 4). The signal from normal aorta was also lower throughout the scans on both day 5 and day 12 in the sham group (day 5: 4.8 ± 0.6 , 4.2 ± 1.1 , 3.4 ± 0.1 , 3.0 ± 0.5 , and 2.5 ± 0.3 %ID/g; day 12: 4.8 ± 0.4 , 4.3 ± 0.2 , 3.7 ± 0.2 , 3.2 ± 0.1 , and 3.0 ± 0.5 %ID/g at 0.5, 3, 6, 16, and 24 h after injection, respectively; $n = 3$; Figs. 2, 3A, 3B, and 4). Taken together, a great enhancement in aortic uptake was achieved in an AAA animal model using ^{64}Cu -NOTA-TRC105-Fab, suggesting its superior efficiency and specificity in CD105 targeting. The signals from normal tissues were similar in AAA, blocking, and sham groups at all time points (Supplemental Fig. 1; supplemental materials are available at <http://jnm.snmjournals.org>), indicating consistent pharmacokinetics of ^{64}Cu -NOTA-TRC105-Fab and accuracy of ROI analysis.

^{64}Cu -NOTA-TRC105-Fab yielded low levels of background signal in the abdominal area, probably because it was mainly cleared through the kidneys (Figs. 2 and 4). The aorta-to-muscle ratio was measured as a standard of imaging contrast. On day 5 and day 12, the aorta-to-muscle ratio was much higher in the AAA group (day 5: 7.3 ± 0.7 , 6.6 ± 0.8 , 7.3 ± 0.9 , 6.0 ± 0.4 , and 5.4 ± 1.0 ; day 12: 8.0 ± 1.8 , 6.5 ± 1.0 , 5.6 ± 1.1 , 5.1 ± 0.9 , and 4.1 ± 0.5 at 0.5, 3, 6, 16, and 24 h after injection, respectively; $n = 3$; Figs. 3C and 3D), compared with the blocking (day 5: 5.4 ± 0.9 , 4.9 ± 0.7 , 4.3 ± 0.8 , 3.8 ± 0.5 , and 2.7 ± 0.2 ; day 12: 4.5 ± 0.8 , 3.5 ± 0.3 , 3.2 ± 0.3 , 2.4 ± 0.2 , and 2.2 ± 0.1 at 0.5, 3, 6, 16, and 24 h after injection, respectively; $n = 3$; Figs. 3C and 3D) and sham groups (day 5: 3.9 ± 1.0 , 3.3 ± 0.9 , 2.7 ± 0.3 , 2.6 ± 0.4 , and 2.1 ± 0.3 ; day 12: 3.4 ± 0.3 , 3.1 ± 0.3 , 2.7 ± 0.2 , 2.5 ± 0.2 ,

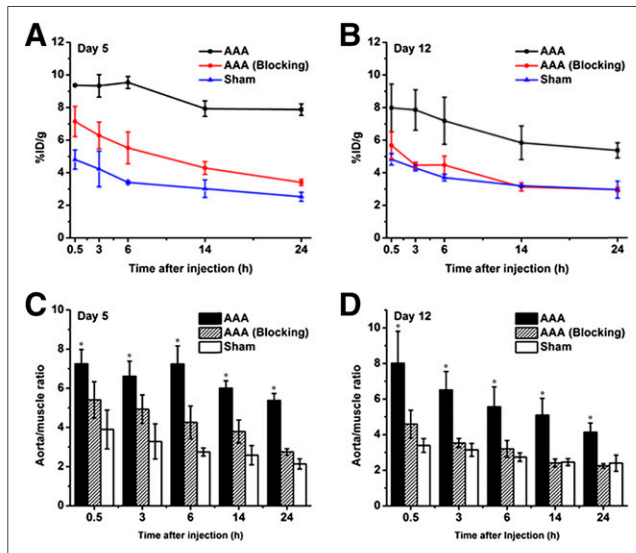


FIGURE 3. ROI analysis of PET images. (A) ^{64}Cu -NOTA-TRC105-Fab uptake (%ID/g) in AAA, blocking, and sham groups, on day 5 after induction. (B) ^{64}Cu -NOTA-TRC105-Fab uptake (%ID/g) in AAA, blocking, and sham groups, on day 12 after induction. (C) Comparison of aorta-to-muscle ratios in AAA, blocking, and sham groups on day 5 after induction. (D) Comparison of aorta-to-muscle ratios in AAA, blocking, and sham groups on day 12 after induction. Differences of aorta uptake and aorta-to-muscle ratio in 3 groups were statistically significant ($P < 0.05$) at all time points ($n = 3$) tested by 1-way ANOVA.

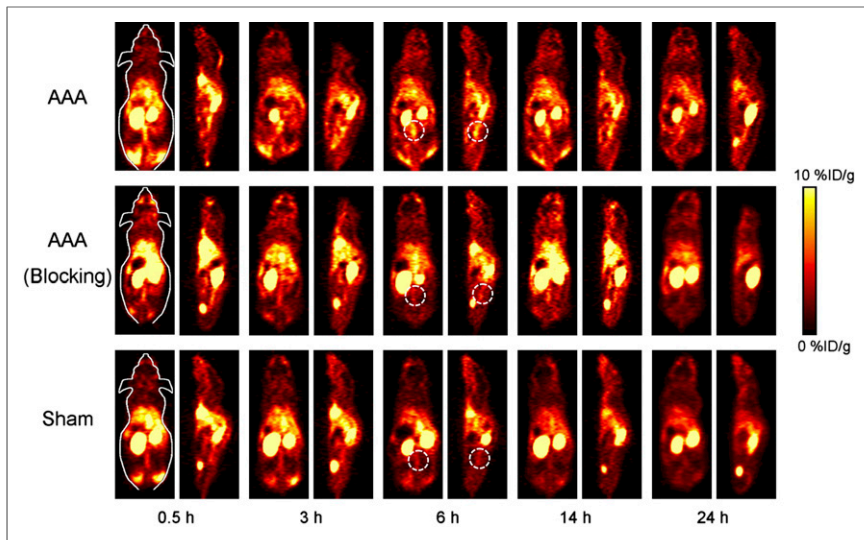


FIGURE 4. In vivo PET imaging on day 12. Serial coronal and sagittal PET images were acquired at different time points after injection of ^{64}Cu -NOTA-TRC105-Fab in AAA-induced mice, AAA-induced mice preinjected with 2 mg of TRC105 (blocking), and sham group without AAA induction on day 12 after induction.

and 2.4 ± 0.4 at 0.5, 3, 6, 16, and 24 h after injection, respectively; $n = 3$; Figs. 3C and 3D). The data clearly demonstrate that excellent imaging contrast can be achieved in AAA with ^{64}Cu -NOTA-TRC105-Fab probe.

To confirm the accuracy of PET images and ROI analysis, mice in all 3 groups were sacrificed at 24 h after injection on day 12. Aorta and other major organs were collected, and the radioactivity signals were measured with a γ counter. The quantitative data from biodistribution and ROI analysis matched well (Fig. 5). Of note, kidney uptake was significantly higher than the liver uptake in the biodistribution study, further validating the renal clearance of ^{64}Cu -NOTA-TRC105-Fab. More important, low uptake observed in the intestine and muscles explains the low background signal and hence superior imaging contrast of ^{64}Cu -NOTA-TRC105-Fab in AAA.

Ex Vivo Imaging and Histology

A macroscopically visible aneurysmal dilation was observed in the abdominal aortas of mice from the AAA group 5 d after induction

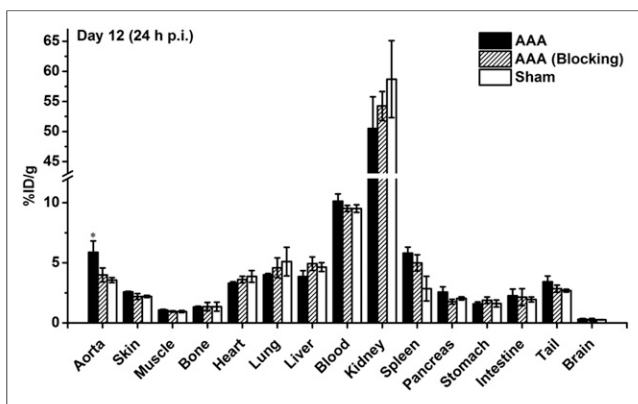


FIGURE 5. Biodistribution of ^{64}Cu -NOTA-TRC105-Fab in AAA, blocking, and sham groups 24 h after injection on day 12 after induction ($n = 3$). p.i. = after administration.

(Supplemental Fig. 2). Ex vivo autoradiography revealed a higher signal in the aortas from the AAA group than the aortas from blocking and sham groups (Fig. 6A), further confirming the accuracy of the results from PET imaging, ROI analysis, and biodistribution studies. Flattening and degradation of the elastic lamina due to increased diameter was obvious in hematoxylin and eosin staining of the dilated aorta (Fig. 6B). The external diameter of the aorta was 0.9 ± 0.1 mm in the AAA group on day 5, whereas it was only 0.4 ± 0.01 mm in the normal aorta.

The intensity of CD105 immunofluorescence was highest on day 5, suggesting active angiogenesis after AAA induction (Fig. 6C). The fluorescence intensity was similar to the normal aorta on day 12. These results correlated well with PET imaging results. Taken together, CD105 was highly expressed in AAA at day 5 after induction, accompanied with structural change of aortic wall, matching well with in vivo and ex vivo studies.

DISCUSSION

In management of AAA, clinicians are often faced with the important decision of whether to perform invasive repair or to manage the condition conservatively. This obstacle arises from the lack of methods that enable the noninvasive acquisition of molecular-cellular information in the developing AAA. Current guidelines recommend endovascular repair or surgery if the aortic diameter exceeds 5.5 cm and follow-up with anatomic imaging every 3–6 mo for aneurysms above 4 cm. However, the size of AAA is neither the sole nor the most accurate determinant for the risk of rupture (31). Individual risk is also influenced by sex, age, smoking, and comorbidities, but its assessment is rarely easy because reliable methods for the optimal evaluation of these variables are not readily available. This situation often leads to difficulties in decision making, and many patients are unnecessarily exposed to the risks of reparative surgery when their aneurysm might never have ruptured if left untreated (32). Serial monitoring of the biologic activity of AAA would be ideal to identify high-risk patients and prompt earlier therapy to prevent rupture while also sparing low-risk patients from expensive and morbid procedures (33).

To date, PET imaging of AAA has been mostly performed with ^{18}F -FDG (5–10,34–37). One disadvantage of ^{18}F -FDG is nonspecific uptake by inflammatory tissues (38), which may lead to false-positive results if there is an inflammatory disease in the artery wall other than AAA. Additionally, the correlation between ^{18}F -FDG uptake in AAA and the chronic inflammation observed in the wall of asymptomatic AAAs is controversial, so metabolic activity of inflammatory cells in asymptomatic AAAs was not sufficient to result in an increased glucose metabolism detectable by ^{18}F -FDG PET (10,39), possibly leading to false-negative results. We also tested the imaging capacity of ^{18}F -FDG in AAA in this study, but we could not detect a significant difference between aortic signals in normal mice and mice with AAA (Supplemental Figs. 3 and 4). On the contrary, the increased expression of CD 105 in AAA could be detected with high sensitivity and specificity using TRC105-Fab. CD105 is expressed on inflamed and some normal tissues to

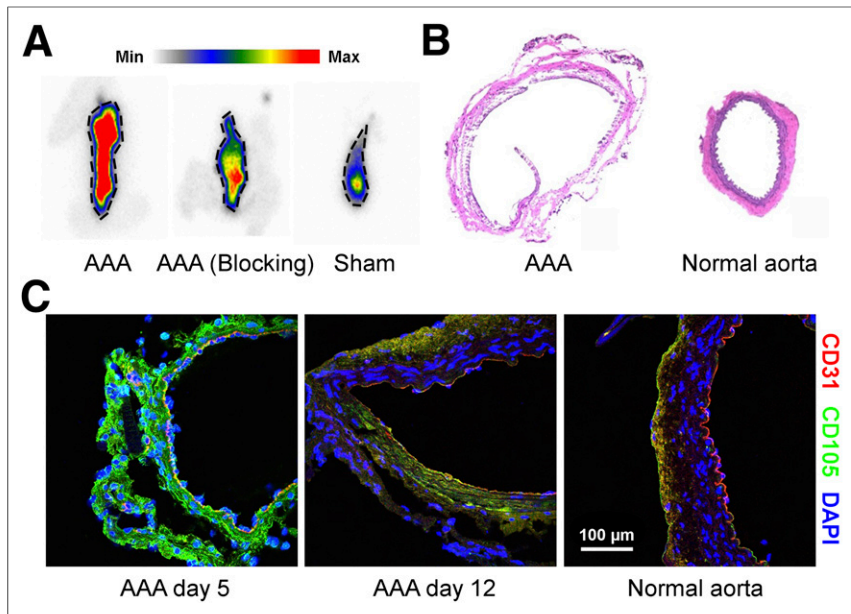


FIGURE 6. Ex vivo analysis. (A) Autoradiography of abdominal aorta from AAA, blocking, and sham groups with ^{64}Cu -NOTA-TRC105-Fab. (B) Hematoxylin and eosin staining of AAA and normal aorta. (C) Immunofluorescence histology of AAA samples collected from AAA group on day 5 and day 12 after induction and normal aorta collected from normal mouse. Red fluorescence indicates CD31 expression, and green fluorescence indicates CD105 expression. Nuclei were counterstained with 4',6-diamidino-2-phenylindole (DAPI). Max = maximum; min = minimum.

a certain extent, but the expression on endothelial cells is significantly higher (40). Therefore, CD105 has been accepted as an important angiogenesis marker (20). ^{64}Cu -NOTA-TRC105-Fab possesses excellent binding efficiency and high targeting specificity toward CD105 as validated by in vitro flow cytometry and in vivo PET imaging in our study. The selective binding ability of the probe may facilitate the differential diagnosis of inflammatory arterial diseases and AAA, therefore preventing false results in PET imaging of AAA.

Antibody-based PET tracers are generally not suitable for AAA imaging because of the hepatic clearance and relatively high intestine uptake, yielding a high background in the abdominal area. However, because of its small size (50–55 kDa), TRC105-Fab was cleared mainly through the renal pathway and taken up minimally by the intestines, as we documented with ex vivo biodistribution studies, providing a superior imaging contrast. TRC105-Fab also had a shorter blood half-life (2.1 h; Supplemental Fig. 5), in comparison with TRC105 (half-life, 3.5 h) (30). However, the blood half-life is still longer than that of small molecules, possibly leading to inaccuracy of AAA uptake. Therefore, more comparative imaging experiments with different targeting probes and imaging modalities are needed in future studies to confirm the potential of TRC105-Fab for PET imaging of AAA.

The limitation to the current preliminary study is the experimental AAA model. Although the murine model has biologic features found in human AAA (28), it does involve aortic dissection as part of the AAA expansion process and may not be ideal to study AAA rupture. Moreover, murine AAA develops over weeks, rather than decades, so the model might not fully represent human AAA in terms of biology and progression (33). Prospective outcome studies are needed first with more clinically relevant animal models of AAA and eventually in patients. These trials will de-

termine whether an increased PET signal, despite the limited spatial resolution of PET, can indeed predict aneurysm rupture.

CONCLUSION

In this study, we demonstrated an increased expression of CD105 in AAA and defined a high-specificity, high-sensitivity probe for the in vivo PET imaging of AAA with TRC105-Fab. More important, we achieved an exquisite imaging contrast because of the low background in the abdominal area. The as-designed imaging probe might open new avenues into AAA research, which will eventually benefit the health care of the whole AAA patient population.

DISCLOSURE

The costs of publication of this article were defrayed in part by the payment of page charges. Therefore, and solely to indicate this fact, this article is hereby marked “advertisement” in accordance with 18 USC section 1734. This work is supported, in part, by the University of Wisconsin–Madison, the Department of Defense (W81XWH-11-1-0644 and W81XWH-11-1-0648), the National Science Foundation (DGE-1256259),

the National Institutes of Health (NIBIB/NCI 1R01CA169365, P30CA014520, 5T32GM08349, and T32CA009206), and the American Cancer Society (125246-RSG-13-099-01-CCE). Charles P. Theuer is an employee of TRACON Pharmaceuticals, Inc. The other authors declare that they have no conflict of interest. No other potential conflict of interest relevant to this article was reported.

REFERENCES

- Belsley SJ, Tilson MD. Two decades of research on etiology and genetic factors in the abdominal aortic aneurysm (AAA): with a glimpse into the 21st century. *Acta Chir Belg.* 2003;103:187–196.
- Nordon IM, Hinchliffe RJ, Loftus IM, Thompson MM. Pathophysiology and epidemiology of abdominal aortic aneurysms. *Nat Rev Cardiol.* 2011;8:92–102.
- Kent KC, Zwolak RM, Jaff MR, et al. Screening for abdominal aortic aneurysm: a consensus statement. *J Vasc Surg.* 2004;39:267–269.
- Hong H, Yang Y, Liu B, Cai W. Imaging of abdominal aortic aneurysm: the present and the future. *Curr Vasc Pharmacol.* 2010;8:808–819.
- Sakalihasan N, Van Damme H, Gomez P, et al. Positron emission tomography (PET) evaluation of abdominal aortic aneurysm (AAA). *Eur J Vasc Endovasc Surg.* 2002;23:431–436.
- Wilkinson MD, Szeto E, Fulham M, Constable CJ, McCaughan BC. FDG positron emission tomographic imaging of a large abdominal aortic aneurysm. *Clin Nucl Med.* 2003;28:130–131.
- Defawe OD, Hustinx R, Defraigne JO, Limet R, Sakalihasan N. Distribution of F-18 fluorodeoxyglucose (F-18 FDG) in abdominal aortic aneurysms: high accumulation in macrophages seen on PET imaging and immunohistology. *Clin Nucl Med.* 2005;30:340–341.
- Reeps C, Essler M, Pelisek J, Seidl S, Eckstein HH, Krause BJ. Increased ^{18}F -fluorodeoxyglucose uptake in abdominal aortic aneurysms in positron emission/computed tomography is associated with inflammation, aortic wall instability, and acute symptoms. *J Vasc Surg.* 2008;48:417–423, discussion 424.
- Truijers M, Kurvers HA, Bredie SJ, Oyen WJ, Blankensteijn JD. In vivo imaging of abdominal aortic aneurysms: increased FDG uptake suggests inflammation in the aneurysm wall. *J Endovasc Ther.* 2008;15:462–467.

10. Kotze CW, Menezes LJ, Endozo R, Groves AM, Ell PJ, Yusuf SW. Increased metabolic activity in abdominal aortic aneurysm detected by ¹⁸F-fluorodeoxyglucose (¹⁸F-FDG) positron emission tomography/computed tomography (PET/CT). *Eur J Vasc Endovasc Surg.* 2009;38:93–99.
11. Barwick TD, Lyons OT, Mikhaeel NG, Waltham M, O'Doherty MJ. ¹⁸F-FDG PET-CT uptake is a feature of both normal diameter and aneurysmal aortic wall and is not related to aneurysm size. *Eur J Nucl Med Mol Imaging.* 2014;41:2310–2318.
12. Vijaynagar B, Bown MJ, Sayers RD, Choke E. Potential role for anti-angiogenic therapy in abdominal aortic aneurysms. *Eur J Clin Invest.* 2013;43:758–765.
13. Chapple KS, Parry DJ, McKenzie S, MacLennan KA, Jones P, Scott DJ. Cyclooxygenase-2 expression and its association with increased angiogenesis in human abdominal aortic aneurysms. *Ann Vasc Surg.* 2007;21:61–66.
14. Choke E, Cockerill GW, Dawson J, et al. Increased angiogenesis at the site of abdominal aortic aneurysm rupture. *Ann N Y Acad Sci.* 2006;1085:315–319.
15. Trollope AF, Golledge J. Angiopietins, abdominal aortic aneurysm and atherosclerosis. *Atherosclerosis.* 2011;214:237–243.
16. Golestani R, Sadeghi MM. Emergence of molecular imaging of aortic aneurysm: implications for risk stratification and management. *J Nucl Cardiol.* 2014;21:251–267, quiz 268–270.
17. Scott DJ, Allen CJ, Honstvet CA, et al. Lymphangiogenesis in abdominal aortic aneurysm. *Br J Surg.* 2013;100:895–903.
18. Orbay H, Zhang Y, Valdovinos HF, et al. Positron emission tomography imaging of CD105 expression in a rat myocardial infarction model with ⁶⁴Cu-NOTA-TRC105. *Am J Nucl Med Mol Imaging.* 2013;4:1–9.
19. Hong H, Severin GW, Yang Y, et al. Positron emission tomography imaging of CD105 expression with ⁸⁹Zr-Df-TRC105. *Eur J Nucl Med Mol Imaging.* 2012;39:138–148.
20. Hong H, Yang Y, Zhang Y, et al. Positron emission tomography imaging of CD105 expression during tumor angiogenesis. *Eur J Nucl Med Mol Imaging.* 2011;38:1335–1343.
21. Zhang Y, Hong H, Engle JW, et al. Positron emission tomography and optical imaging of tumor CD105 expression with a dual-labeled monoclonal antibody. *Mol Pharm.* 2012;9:645–653.
22. Zhang Y, Hong H, Orbay H, et al. PET imaging of CD105/endoglin expression with a ⁶¹/⁶⁴Cu-labeled Fab antibody fragment. *Eur J Nucl Med Mol Imaging.* 2013;40:759–767.
23. Andrew SM, Pimm MV, Perkins AC, Baldwin RW. Comparative imaging and biodistribution studies with an anti-CEA monoclonal antibody and its F(ab)₂ and Fab fragments in mice with colon carcinoma xenografts. *Eur J Nucl Med.* 1986;12:168–175.
24. Chen F, Nayak TR, Goel S, et al. In vivo tumor vasculature targeted PET/NIRF imaging with TRC105(Fab)-conjugated, dual-labeled mesoporous silica nanoparticles. *Mol Pharm.* 2014;11:4007–4014.
25. Hong H, Yang K, Zhang Y, et al. In vivo targeting and imaging of tumor vasculature with radiolabeled, antibody-conjugated nanographene. *ACS Nano.* 2012;6:2361–2370.
26. Zhang Y, Hong H, Severin GW, et al. ImmunoPET and near-infrared fluorescence imaging of CD105 expression using a monoclonal antibody dual-labeled with ⁸⁹Zr and IRDye 800CW. *Am J Transl Res.* 2012;4:333–346.
27. Hong H, Zhang Y, Severin GW, et al. Multimodality imaging of breast cancer experimental lung metastasis with bioluminescence and a monoclonal antibody dual-labeled with ⁸⁹Zr and IRDye 800CW. *Mol Pharm.* 2012;9:2339–2349.
28. Yamanouchi D, Morgan S, Stair C, et al. Accelerated aneurysmal dilation associated with apoptosis and inflammation in a newly developed calcium phosphate rodent abdominal aortic aneurysm model. *J Vasc Surg.* 2012;56:455–461.
29. Hong H, Zhang Y, Nayak TR, et al. Immuno-PET of tissue factor in pancreatic cancer. *J Nucl Med.* 2012;53:1748–1754.
30. Yang Y, Zhang Y, Hong H, Liu G, Leigh BR, Cai W. In vivo near-infrared fluorescence imaging of CD105 expression during tumor angiogenesis. *Eur J Nucl Med Mol Imaging.* 2011;38:2066–2076.
31. Sakalihan N, Hustinx R, Limet R. Contribution of PET scanning to the evaluation of abdominal aortic aneurysm. *Semin Vasc Surg.* 2004;17:144–153.
32. Nahrendorf M, Keliher E, Marinelli B, et al. Detection of macrophages in aortic aneurysms by nanoparticle positron emission tomography-computed tomography. *Arterioscler Thromb Vasc Biol.* 2011;31:750–757.
33. Kitagawa T, Kosuge H, Chang E, et al. Integrin-targeted molecular imaging of experimental abdominal aortic aneurysms by ¹⁸F-labeled Arg-Gly-Asp positron-emission tomography. *Circ Cardiovasc Imaging.* 2013;6:950–956.
34. English SJ, Piert MR, Diaz JA, et al. Increased ¹⁸F-FDG uptake is predictive of rupture in a novel rat abdominal aortic aneurysm rupture model. *Ann Surg.* 2015;261:395–404.
35. Menezes LJ, Kotze CW, Hutton BF, et al. Vascular inflammation imaging with ¹⁸F-FDG PET/CT: when to image? *J Nucl Med.* 2009;50:854–857.
36. Morbelli S, Ghigliotti G, Spinella G, et al. Systemic vascular inflammation in abdominal aortic aneurysm patients: a contrast-enhanced PET/CT study. *Q J Nucl Med Mol Imaging.* 2014;58:299–309.
37. Palombo D, Morbelli S, Spinella G, et al. A positron emission tomography/computed tomography (PET/CT) evaluation of asymptomatic abdominal aortic aneurysms: another point of view. *Ann Vasc Surg.* 2012;26:491–499.
38. Courtois A, Nusgens BV, Hustinx R, et al. ¹⁸F-FDG uptake assessed by PET/CT in abdominal aortic aneurysms is associated with cellular and molecular alterations prefacing wall deterioration and rupture. *J Nucl Med.* 2013;54:1740–1747.
39. Tegler G, Ericson K, Sorensen J, Bjorck M, Wanhainen A. Inflammation in the walls of asymptomatic abdominal aortic aneurysms is not associated with increased metabolic activity detectable by ¹⁸F-fluorodeoxyglucose positron-emission tomography. *J Vasc Surg.* 2012;56:802–807.
40. Middleton J, Americh L, Gayon R, et al. A comparative study of endothelial cell markers expressed in chronically inflamed human tissues: MECA-79, Duffy antigen receptor for chemokines, von Willebrand factor, CD31, CD34, CD105 and CD146. *J Pathol.* 2005;206:260–268.